Non-Fullerene Acceptor for Organic Solar Cells with Chlorination on Dithieno[3,2-b:2′,3′-d]pyrrol Fused-Ring

Chlorination on Dithieno[3,2-*b*:2′,3′-*d*]pyrrol Fused-Ring Non-Fullerene Acceptor for Organic Solar Cells

Renyong Geng,[†,#] Xin Song,[‡,#] Haohao Feng,[†] Jiangsheng Yu,[Π] Ming Zhang,[§] Nicola Gasparini,[‡] Zhuohan Zhang,[†] Feng Liu,*[,§] Derya Baran,*[,‡] and Weihua Tang*[,†]

[†]School of Chemical Engineering, Nanjing University of Science and Technology, Nanjing 210094, China
[‡]KAUST Solar Center (KSC), King Abdullah University of Science and Technology (KAUST), Thuwal 23955-6900, Saudi Arabia
[Π]MIIT Key Laboratory of Advanced Solid Laser, Nanjing University of Science and Technology, Nanjing 210094, China
[§]Department of Physics and Astronomy, Collaborative Innovation Center of IFSA, Shanghai Jiao Tong University, Shanghai 200240, China

ABSTRACT: A narrow bandgap molecular acceptor, **IPIC-4Cl**, featuring an indacenobis(dithieno[3,2-*b*:2′,3′-*d*]pyrrol) (INP) core with 2-butyl-1-octyl sidechains and chlorinated (dicyanomethylidene)-indan-1-one (IC) as electron-accepting endgroup, has been rationally designed as non-fullerene acceptors (NFAs) for organic solar cells (OSCs). The impact of chlorination on the acceptor unit is revealed by a comparison study with two counterpart NFAs bearing fluorinated or non-halogenated IC unit. The synergetic photophysical and morphological analyses reveal that PBDB-T:**IPIC-4Cl** blend possesses efficient exciton dissociation and charge collection integrated with higher crystallinity and optimized phase separation. Consequently, the OSCs constructed by PBDB-T:**IPIC-4Cl** obtain a champion power conversion efficiency (PCE) of 13.4% with an extremely low energy loss of 0.51 eV. More encouragingly, we achieve a higher photovoltaic performance of 14.3% for ternary solar cells by using a combination of optimal amount of $PC_{71}BM$ with PBDB-T:IPIC-4Cl blend.

TOC

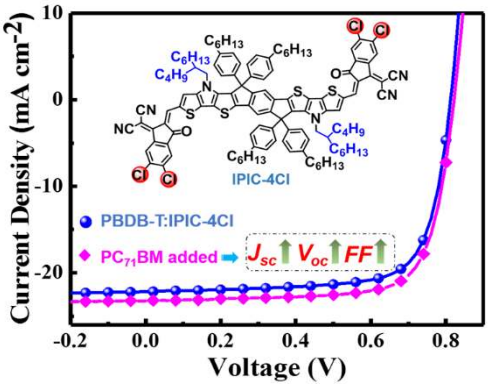

Organic solar cells (OSCs) have emerged as one of the promising photovoltaic technology, owing to their superior performance and capacity for low-cost and scalable solution-processing fabrication. [1-6] In comparison with traditional fullerene-based electron acceptor, the non-fullerene acceptors (NFAs) with acceptor-donor-acceptor (A-D-A) structure exhibited significant advantages, such as variability of energy levels and

absorption range, strong absorption strength and adjustable chemical structure. Among the families of NFA small molecule, the fused-ring electron-acceptors (FREAs) have achieved dramatic progress in realizing high-performance bulk-heterojunction (BHJ) OSCs.[7-14] The power conversion efficiencies (PCEs) of the single-junction OSCs based on FREAs were boosted to 15.7 % as a result of optimization of the central core units, electron-withdrawing terminal groups, and the sidechain in core units.[15-18] Moreover, in combination with tandem cell architecture, the photovoltaic performance containing FREAs can further be improved to over 17%.[19]

Rational design and synthesis of novel FREA as well as relationship of their structure-to-performance (especially the energetic loss (E_{loss}, $E_{loss} = E_g^{opt} - eV_{oc}$, E_g^{opt}: opticl bandgap, V_{oc}: open-circuited voltage) *vs* the short-circuited current densities (J_{sc})) are indispensable to develop highly efficient OSCs for real-world application.[20-22] Summarizing the literature about FREA, benefitting from the well-balanced feature between open-circuited voltage (V_{oc}) and J_{sc}, FREA material with bandgap between 1.45 eV and 1.7 eV are more promising to yield impressive PCEs.[23-27] In contrast, many of the near-infrared bandgap FREAs (E_g<1.45 eV) usually showed a high J_{sc} with a sacrificed voltage (the high E_{loss} values), which resulted in a moderate PCEs. [28-31] Encouragingly, our group developed a new FREA material named INPIC-4F with 5,5,12,12-tetrakis(4-hexylphenyl)-indacenobis(dithieno[3,2-*b*:2′,3′-*d*]pyrrol) (INP) as a novel building block endcapped by fluorinated 3-(dicyanomethylidene)-indan-1-one (IC). [32-34] This NFA exhibits broad and strong absorption in 600-900 nm region with an optical bandgap of 1.39 eV. Thanks to the favorable crystallinity and well-defined

bicontinuous network in blend films, INPIC-4F based devices showed an excellent PCE (13.13%) with low E_{loss} (ca. 0.54 eV) in binary devices by blending with PBDB-T (the start-of-the-art polymer donor). Despite INPIC-4F presented the absorption onset of 900 nm, the solar spectrum in 900-1100 nm range is still absent, indicating the improvement room to harvest more photons matching the solar flux in the NIR region.[35] Therefore, it is urgent and a challenge to design novel NIR FREAs matching with polymer donors to further improve the J_{sc} and PCE by simultaneously maintaining the extremely low E_{loss}.

Compared to the fluorination strategy we mentioned above, the chlorinated terminal units possess a more red-shifted absorption window, enhanced crystallinity and better device photostability, which is due to their stronger intramolecular charge-transfer (ICT) effect. [17,18,36] In addition, the Cl substitutes are easier to synthesize than that of F counterparts, which reduced the cost of the photovoltaic materials and made them more suitable for practical application. On the other hand, employing multiple light-absorbing materials to broaden the absorption spectrum has been employed as a promising approach to realize high-performance in organic solar cells.[37] Recently, Zhu, Ding and Chen et al reported that by using fullerene derivative as a combinatory acceptor with polymer donor:non-fullerene acceptor pair can be advantageous, as $PC_{61}BM$ or $PC_{71}BM$ can be functioned as good electron-transporting channel and solid processing-aid, [19,38] while NFA material possesses wide absorption window and highly tunable energy-level alignment. Via combination of these three component and the suitable blend morphology, it thus may be a judicious choice to construct high-

performance organic solar cells.

In this contribution, we combined the strategy discussed above (chlorination and ternary system) together and reported a highly efficient ternary system with PCE over 14%. Indeed, three INP based NFAs (**IPIC-4Cl**, **IPIC-4F** and **IPIC**, **Figure** 1a) with/without halogen-substituted terminal block (-Cl, -F, -H) were synthesized and studied systematically. Compared to **IPIC**, **IPIC-4Cl** and **IPIC-4F** exhibit narrower bandgaps and downshifted energy levels (both the highest occupied molecular orbital (HOMO) and lowest unoccupied molecular orbital (LUMO)). When blended with a state-of-the-art polymer donor (PBDB-T) featuring complementary absorption with our as-developed NFAs, three acceptors derived blend films show explicit differences in light-harvesting capacity, charge transport ability and morphology. The **IPIC-4Cl** based BHJ blend films exhibit a broad absorption range (300 nm-900 nm) and more balanced charge mobilities (μ_h/μ_e = 1.26), resulting in higher J_{SC} and FF values for the OSCs than those of **IPIC-4F** and **IPIC**-based devices. Furthermore, **IPIC-4Cl** features enhanced ICT effect and molecular packing in comparison with other two counterparts. Consequently, the **IPIC-4Cl** based OSCs enabled suppressed trap-assisted recombination, increased carrier density and improved carrier generation and extraction efficiencies. Indeed, the PBDB-T:**IPIC-4Cl** based binary OSCs exhibited superior efficiency of 13.4%. When adding $PC_{71}BM$ functioned as the phase mediator and electron-transporting channel into PBDB-T:**IPIC-4Cl** blend, the OSCs show an impressive PCE of 14.3%. (Table S9&S10 in Supporting Information) These results strongly prove that our FREA molecular design strategy and further combination of

$PC_{71}BM$ as a combinatory acceptor are effective for the construction of high-performance OSCs.

We want to note that the direct Cl-F replacement on INPIC-4F could only obtain a poorly soluble material (**INPIC-4Cl**, Scheme S1), hence branched 2-butyl-1-octyl (BO) sidechains were rationally introduced on INP core to achieve solution-processable NFAs for solution-processing OSCs.[39] In order to allow us to accurately understand the effect of endgroup substitution on device performance, we keep this branched sidechain above INP core unit the same length. Thus, a series of FREA based on INP core unit with BO sidechain (IPIC-4Cl, IPIC-4F and IPIC) were successfully synthesized by Knoevenagel condensation between INP di-aldehyde and different IC derivatives with 69~80% yields (Figure 1a). The detailed synthesis and structural characterization including ^{1}H NMR, ^{19}F NMR, ^{13}C NMR and mass spectra are provided in Supporting Information (Figure S1-S8). All three acceptors exhibited good solubility in common solvents, such as chlorobenzene (CB), chloroform (CF) and 1,2-dichlorobenzene (DCB). In addition, **IPIC-4Cl**, **IPIC-4F** and **IPIC** show good thermal stability, with the decomposition temperature (T_d, 5 % weight-loss temperature) of 377 ℃, 365 ℃ and 358 ℃, respectively (Figure S9a).[40]

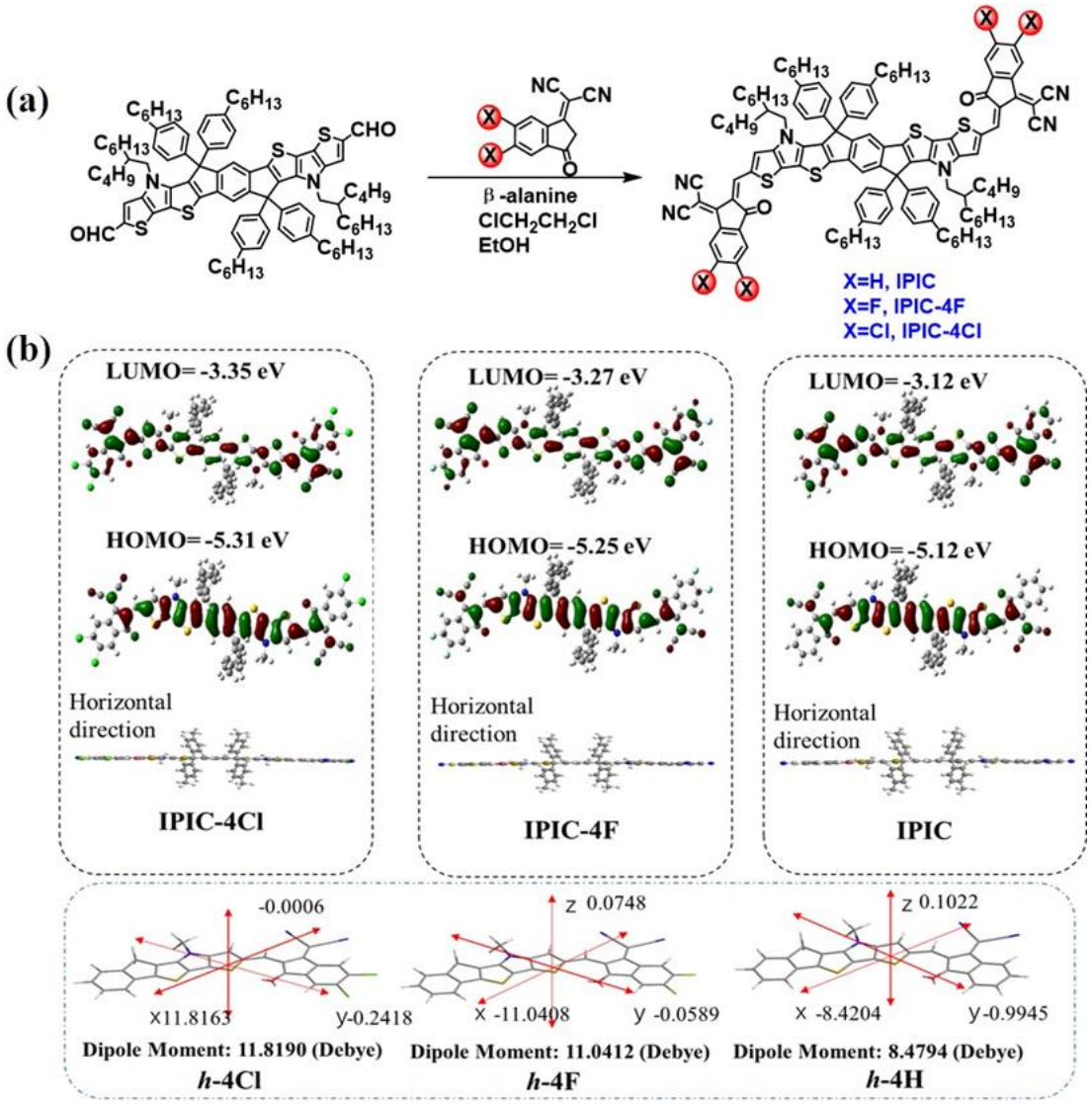

Figure 1. (a) Synthetic route for three NFAs; (b) the simulated frontier molecular orbits of the NFAs and the dipole moments of the corresponding structurally simplified acceptors.

Density functional theory (DFT) calculation with B3LYP/6-31G (d, p) basis set was performed to investigate the chemical geometry of three NFAs.[41] As shown in Figure 1b, all three molecules show nearly planar backbone configurations and similar wave function distributions in frontier orbitals, i.e., the electron density of HOMO is mainly localized on donor segment whereas the electron density of LUMO delocalized over the entire conjugated backbone. The halogenated NFAs (**IPIC-4Cl/IPIC-4F**) exhibit narrower bandgap and down-shifted LUMO energy levels, agreeing with the optical

and CV results. To evaluate the influence of different terminal atoms (-Cl, -F, -H) on the strength of intramolecular interaction, the dipole moment (δ) was calculated based on half of the molecules as models (marked as *h*-4H, *h*-4F, *h*-4Cl as shown in Figure 1b). The *h*-4Cl shows larger dipole moment value (δ=11.82 Debye) than *h*-4F (δ=11.04 Debye) and *h*-4H (8.47 Debye), indicating the occurrence of enhanced ICT effect in **IPIC-Cl**.[17,42]

The absorption and electrochemical properties of IP-series FREA materials are summarized in Table 1. As depicted in Figure S9b, halogenated acceptors featured higher extinction coefficients (2.90×10^5 M^{-1} cm^{-1} for **IPIC-4Cl** and 2.96×10^5 M^{-1} cm^{-1} for **IPIC-4F**, respectively) than that of **IPIC** (2.32×10^5 M^{-1} cm^{-1}). Moreover, the optical bandgap (E_g^{opt}) calculated from the absorption onset for **IPIC-4Cl** was 1.32 eV, while 1.38 eV and 1.44 eV was calculated for **IPIC-4F** and **IPIC**, respectively. Cyclic voltammetry (CV) experiments were further performed to evaluate the molecular energy levels for three acceptors (Figure S9c). As calculated from the onset of oxidative and reductive peaks of CV curves, the HOMO and LUMO levels of **IPIC-4Cl** were examined as -5.51 eV/-3.95 eV, while -5.54 eV/-3.94 eV and -5.47 eV/-3.82 eV were calculated for **IPIC-4F** and **IPIC** (Figure 2b), respectively. Compared to **IPIC-4F**, **IPIC-4Cl** possesses slightly down-shifted HOMO but up-lifted LUMO levels, which is constant with the trend calculated by optical bandgap (Table 1).

The photovoltaic performance of IPIC-series as electron acceptors was evaluated by incorporating PBDB-T as electron donor. The OSCs were constructed with a conventional configuration: ITO/ PEDOT:PSS(~30 nm)/active layer(~120 nm)/(2-

(1,10-phenanthrolin-3-yl)naphth-6-yl)diphenylphosphine oxide (Phen-NaDPO) (~8 nm)/Ag(~100 nm) (Figure 2c). Detailed device fabrication and optimization conditions, such as donor/acceptor weight ratio, additive volume ratio, and thermal annealing temperature are provided in the Supporting Information (Table S1-S7). In detail, chlorobenzene (CB) was used as the processing solvent. In all three blend solutions with donor: acceptor blend weight ratio of 1:1, 0.5 % (*v/v*) 1,8-diiodooctane (DIO) was added as processing additive. After spin-coating the blend solution onto the ITO/PEDOT:PSS substrate, the thermal annealing at 100 °C for 10 min is crucial to obtain optimal photovoltaic performance, especially for the FF.

Table 1. Optical, electrochemical and thermal properties of three NFAs

Acceptor	λ_{max} [nm][a)]	λ_{max} [nm][b)]	λ_{onset} [nm][b)]	E_g^{opt} [eV][c)]	HOMO [eV]	LUMO [eV]	E_g^{CV} [eV]	T_d [°C]
IPIC-4Cl	790	855	939	1.32	-5.51	-3.95	1.56	377
IPIC-4F	776	824	899	1.38	-5.54	-3.94	1.60	365
IPIC	761	776	861	1.44	-5.47	-3.82	1.65	358

[a)] In chloroform solution (~ 10^{-5} M); [b)] in thin film; [c)] $E_g^{opt} = 1240/\lambda_{onset}$.

The current-voltage (*J*-*V*) characteristics of the optimized devices with three acceptors are presented in Figure 2d, with the corresponding photovoltaic parameters listed in Table 2. The photovoltaic performance of binary devices derived from halogenated acceptors were significantly improved along with increasing J_{SC} and FF, compared to **IPIC** devices. Indeed, upon introduction of fluorine atoms in the endgroup (**IPIC-4F**), the J_{SC}, FF and PCE increased from 7.16 mA cm^{-2} to 19.8 mA cm^{-2}, from 58.6% to 67.1% and from 3.98% to 11.1%, respectively. Furthermore, the optimized **IPIC-4Cl** based OSC was increased to 13.4% with a significantly enhanced J_{sc} value

of 22.2 mA cm^{-2} and FF of 74.0%, and V_{oc} of 813 mV. More encouragingly, the E_{loss} value obtained from **IPIC-4Cl** based device decreased to 0.51 eV, which is lower than most of representative chlorinated NFAs ones in literature (Table S9). According to the literature reported, the $PC_{71}BM$ can function as electron transport channel and solid processing-aid, which would significantly improve the performance by adding $PC_{71}BM$ as the third component in OSCs. [37,43,44] To further enhance the photovoltaic performance of PBDB-T:IPIC-4Cl system, we introduced the $PC_{71}BM$ as the third component to construct the ternary devices. Successfully, as shown in Figure 2d, the optimized PBDB-T:**IPIC-4Cl**:$PC_{71}BM$ (1:1:0.3, in weight ratio) device showed a maximum PCE of 14.3% with a higher J_{sc} of 23.3 mA cm^{-2}, a V_{OC} of 822 mV, and an FF of 74.6%. The functions of $PC_{71}BM$ in these devices is systemically investigated by transient photocurrent (TPC) and photo-induced charge carrier extraction using linearly increasing voltage (Photo-CELIV) characterizations. As demonstrated in Figure S10a and 10b, the measured carrier concentration and carrier mobility in optimized $PC_{71}BM$-added devices are higher than those of binary blends, indicating more efficient carrier generation and transport achieved in PBDB-T:**IPIC-4Cl**:$PC_{71}BM$ (1:1:0.3) devices, which induced a higher J_{sc} and FF in ternary system in comparison with that of binary device.[38]

The external quantum efficiency (EQE) spectra were investigated to verify the higher J_{sc} value for the PBDB-T:IPIC-4Cl- based devices. As depicted in Figure 2e, the **IPIC-4Cl** devices showed wider and stronger photocurrent responses (over 60% of EQE value across the range of 450 nm-800 nm) compared to the **IPIC** and **IPIC-4F** devices.

Moreover, compared to the binary system (PBDB-T:IPIC-4Cl), the addition of $PC_{71}BM$ induced the EQE values over 70% in the range of 500 nm to 700 nm. In general, the high EQE curve should be related to the optimal carrier dynamic factors and morphology of the blend films. The possible reasons for higher photocurrent response in ternary system are as follows: 1): A higher absorption coefficient of ternary film was observed in comparison with that of binary system, which is beneficial for the use of solar light (Figure S9d); 2) higher carrier concentration and mobility may cause the higher carrier transport and extraction capability, thus resulting in a higher EQE values; 3) the blend morphology was further optimized after incorporating $PC_{71}BM$ into binary system.[38] (the details will be discussed below).

To investigate the exciton dissociation and charge collection properties of these IPIC series-based devices. We characterized the variations of photocurrent density (J_{ph}) as a function of effective voltage (V_{eff}) (presented in Figure 2f). In detail, J_{ph} is calculated from $J_{ph} = J_l - J_d$, where J_l and J_d are the current density under illumination at 100 mW cm^{-2} and in the dark, respectively. V_{eff} is given by $V_{eff} = V_0 - V$, where V_0 is the compensation voltage defined as J_{ph} (V_0)=0, and V is the applied voltage.[45] Obviously, **IPIC-4Cl** and **IPIC-4F** based devices achieved high J_{ph} even at low V_{eff}, and both the devices reached the saturation current density (J_{sat}) when V_{eff} is lower than 1 V, whereas the PBDB-T:IPIC devices depicted a strong dependence of J_{ph} with V_{eff}, the carriers were still not under saturation condition when V_{eff} was higher than 2.0 V, demonstrating that the severe recombination processes and limited charge extraction are observed in IPIC based devices.[46] J_{ph}/J_{sat} values were also calculated to evaluate the

processes of exciton dissociation in these devices.[47] The J_{ph}/J_{sat} values of **IPIC-4Cl** and **IPIC-4F** based devices were 94.2% and 91.4%, respectively, while the photocurrent density in **IPIC** based devices couldn't reach to saturation condition. A higher J_{ph}/J_{sat} value of **IPIC-4Cl** based device suggests higher exciton dissociation and more efficient charge collection realized with the chlorinated NFAs.[48]

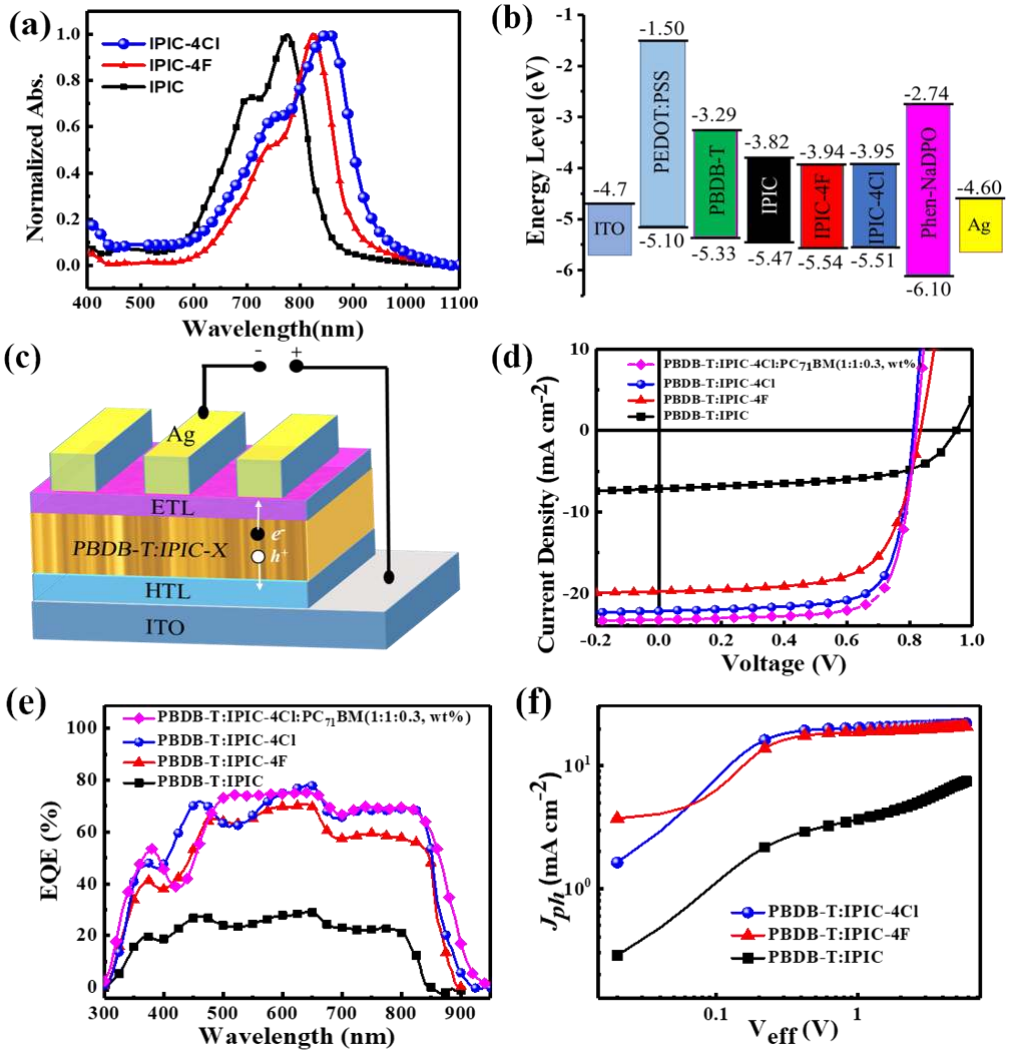

Figure 2. (a) UV-Vis-NIR absorption spectra of three acceptors in thin films;(b) Energy levels of corresponding materials; (c) Schematic diagram of device structure; (d) *J-V* curves under AM 1.5 G illumination; (e) EQE plot of the corresponding optimized devices; (f) J_{ph} versus V_{eff} of designed devices.

Light intensity (P) dependence of J_{sc} and V_{oc} were plotted to evaluate the recombination processes in the binary OSCs.[49] Normally, the relationship of P and J_{sc}

can be defined as $J_{sc} \propto P^S$, and the bimolecular recombination in the devices are negligible when S value is close to 1.[50] As shown in Figure 3a, the slope for **IPIC-4Cl** and **IPIC-4F** devices is 0.995 and 0.996, respectively, indicating that the bimolecular recombination is not the main limiting factor of carrier recombination in the two systems mentioned above.[29] Compared to halogenated NFA based devices, the S value of 0.968 for **IPIC** based device suggests severe bimolecular recombination in PBDB-T:**IPIC** blends. Now we shined light into the relationship of V_{oc} as a function of light intensities (Figure 3b), which transfer the information of trap-assisted recombination. In principle, a slope approximately in the order of kT/q is a signal that bimolecular recombination is dominant, while a stronger dependence of V_{oc} on P_{light} with a slope of 2 kT/q is identified that trap-assisted recombination become severe. [51] Owing to the better phase separation and molecular packing (will discuss in morphology part), the slope of **IPIC-4Cl** based devices was decreased to 1.16 kT/q, slightly lower than that of PBDB-T:**IPIC-4F** blend film (1.21 kT/q) and significantly lower than that of **IPIC** based devices (1.95 kT/q). The results indicate that the trap-assisted recombination was suppressed in the two halogenated NFA based devices, especially for PBDB-T:**IPIC-4Cl** blends.[52] We further utilize the same characterization for the ternary devices (PBDB-T:IPIC-4Cl:$PC_{71}BM$) because of the slight higher J_{sc} and FF than that of binary devices (PBDB-T:IPIC-4Cl), which partly associated with the recombination behavior. As depicted in Figure S10c&S10d, the slope of J_{sc} vs light intensity are nearly same for binary and ternary system, while the slope for ternary device is little lower than that of binary system when we plotted the V_{oc} vs light intensity values. Such results indicate

that the more efficient suppressed trap-assisted recombination was achieved by combining the chlorination and ternary blend strategy.

Table 2. Device performance parameters of OSC based on PBDB-T and NFAs

Active layer (by weight ratio)	J_{sc} [mA cm^{-2}]	J_{sc} [a)] [mA cm^{-2}]	V_{oc} [mV]	FF [%]	PCE [%]	PCE [b)] [%]
PBDB-T:IPIC (1:1)	7.16	6.93	950	58.6	3.98	3.81
PBDB-T:IPIC-4F (1:1)	19.8	18.8	835	67.1	11.1	10.7
PBDB-T:IPIC-4Cl (1:1)	22.2	21.2	813	74.0	13.4	13.0
PBDB-T:IPIC-4Cl:PC$_{71}$BM (1:1:0.1)	22.6	21.3	823	73.2	13.6	13.4
PBDB-T:IPIC-4Cl:PC$_{71}$BM (1:1:0.3)	23.3	21.8	822	74.6	14.3	14.1
PBDB-T:IPIC-4Cl:PC$_{71}$BM (1:1:0.5)	20.4	19.5	822	72.3	12.1	11.8

[a)] J_{sc} integrated from EQE curves in Figure 2b; [b)] average PCEs from 10 devices.

To further understand the charge transport properties of IPIC series-based devices, the hole and electron mobilites (μ_h and μ_e) of these blend films were calculated by space-charge-limited-current (SCLC) method (Figure 3c and 3d). The PBDB-T:**IPIC-4Cl** blend films present higher and more balanced charge mobilities (μ_h = 1.26×10^{-4} cm^2 V^{-1}·s^{-1}, μ_e = 1.00×10^{-4} cm^2 V^{-1}·s^{-1} and μ_h/μ_e = 1.26), compared to those of PBDB-T:**IPIC-4F** films (μ_h = 1.22×10^{-4} cm^2 V^{-1}·s^{-1}, μ_e = 5.61×10^{-5} cm^2 V^{-1}·s^{-1} and μ_h/μ_e = 2.17) and PBDB-T:**IPIC** films (μ_h = 5.72×10^{-5} cm^2 V^{-1}·s^{-1}, μ_e = 2.53×10^{-7} cm^2 V^{-1}·s^{-1} and μ_h/μ_e = 226) (Table S8). Therefore, an enhanced and balanced charge mobility after the Cl atoms incorporation is beneficial to suppress charge recombination in IPIC-4Cl devices. The further carrier extraction dynamics observation was examined by the TPC characterization. As the **IPIC-4Cl** based OSCs show an improved charge density than **IPIC-4F** and **IPIC** devices (Figure S10c), which is consistent with the higher J_{SC}

observed for the corresponding **IPIC-4Cl** OSCs. Moreover, the IPIC-4Cl based devices featured a smaller charge extraction time in comparison with that of IPIC-4F and IPIC-based devices (Figure S10d). Totally, the higher charge transport and extraction are one of the main reasons for the higher FF and PCE in PBDB-T:**IPIC-4Cl** OSCs.

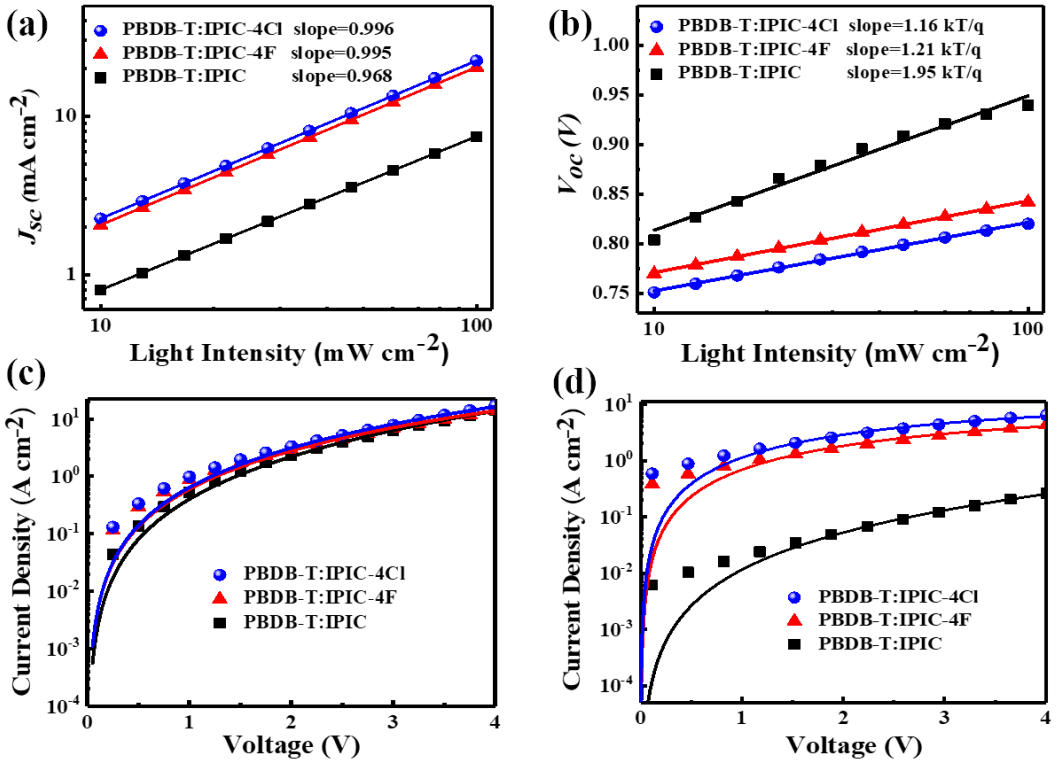

Figure 3. (a) J_{sc} versus light intensity of designed devices;(h) V_{oc} versus light intensity of designed devices; (c) Hole mobility plots from SCLC measurement; (d) Electron mobility plots from SCLC measurement.

To correlate the optoelectronic properties, device performance with molecular structural information and to understand the chlorination effect on a molecular level, grazing incidence wide angle X-ray scattering (GIWAXS) was performed for the neat acceptor materials and donor: acceptor blend films. The corresponding GIWAXS patterns were presented in Figure S11 and Figure 4. As depicted, **IPIC-4Cl** and **IPIC-4F** films exhibit quite strong structure order, with more pronounced (100) diffraction (at 0.32 Å^{-1} for **IPIC-4Cl** and 0.29 Å^{-1} for **IPIC-4F**) in in-plane (IP) orientation and

strong π–π stacking (at 1.82 $Å^{-1}$ for **IPIC-4Cl** and 1.92 $Å^{-1}$ for **IPIC-4F**) in out-of-plane (OOP) direction, suggesting that halogenated acceptors have a preferred face-on orientation with respect to the substrate.[45] In contrast, the **IPIC** pure film exhibits a broad (100) diffraction at 0.33 $Å^{-1}$ and π–π stacking peak at ≈ 1.95 $Å^{-1}$, indicative of its relatively weak crystallinity and disordered packing. The π–π stacking distance ($d_{\pi-\pi}$) was evaluated to quantize the crystallinity, and we found that **IPIC-4Cl** neat film has the smallest $d_{\pi-\pi}$ of 3.45 Å. This indicates that **IPIC-4Cl** exhibits the strongest intermolecular aggregations, which is constant with the largest redshift in the absorption spectrum of pure film. Further considering about the blend films, the strong π-π stacking peaks in the OOP direction of three blend films (located at 1.74 $Å^{-1}$, 1.75 $Å^{-1}$, 1.77 $Å^{-1}$, corresponding to $d_{\pi-\pi}$ of ~3.61Å, 3.59 Å, 3.54 Å for **IPIC-4Cl**, **IPIC-4F**, **IPIC**, respectively), demonstrating that IPIC-4Cl blend film preferred a more intense molecular packing. [47] The phase separation of three blend films was further investigated by Resonant Soft X-ray scattering (R-SoXS) measurements. As R-SoXS profiles shown in Figure 4e, three binary blends showed distinguishing phase separation for **IPIC-4Cl**, **IPIC-4F** and **IPIC** respectively. Small domains in PBDB-T:**IPIC-4Cl** film indicated more D:A interfaces are produced in blend film to efficiently facilitate exciton separation, [53] which contributes to the high J_{sc} values for the binary devices. In addition to the GIWAXS and R-SoXS measurements, high-resolution transmission electron microscope (TEM) and atomic force microscopy (AFM) technology were also utilized to directly reveal the blend morphology. As shown in Figure S12, an apparent aggregation feature of PBDB-T:**IPIC-4Cl** blend films was observed and the root-

meant-square roughness (RMS) was increased to ca. 2.81 nm. In contrast, the **IPIC** and **IPIC-4F** based films is featureless with lower roughness value. Such optimized morphology of **IPIC-4Cl** film is beneficial for charge generation and charge transport,[54] supporting their higher J_{sc} and FF and better PCE in comparison with those of **IPIC** and **IPIC-4F** film.

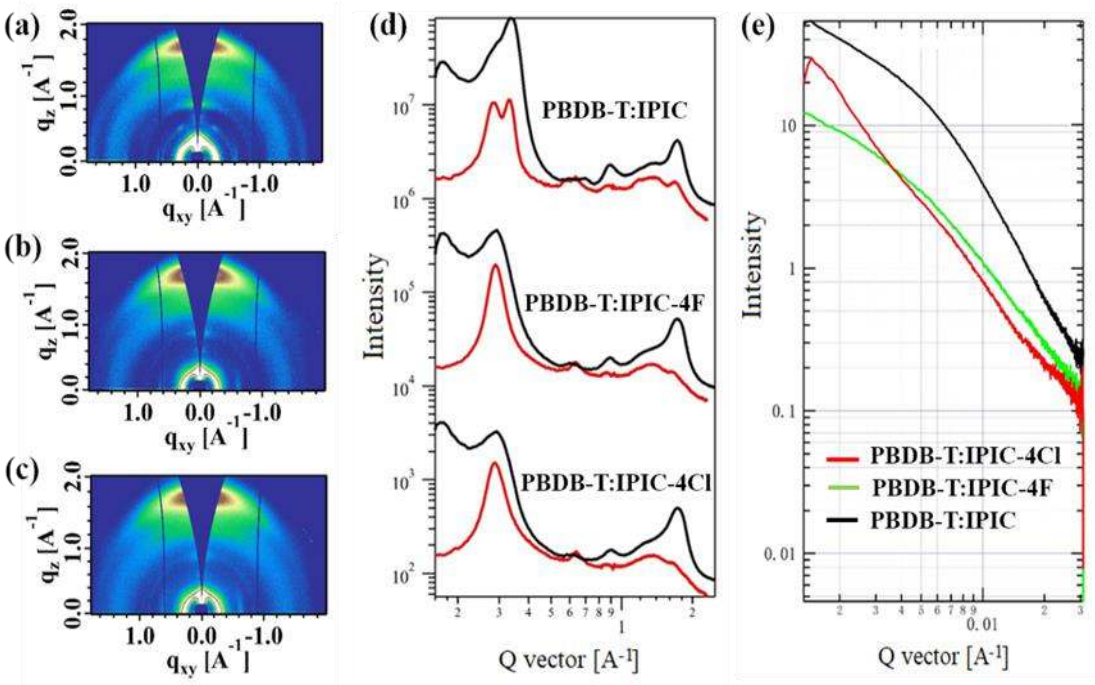

Figure 4. GIWAXS of blend films: (a) PBDB-T:IPIC, (b) PBDB-T: IPIC-4F, (c) PBDB-T:IPIC-4Cl. (d) In-plane (red line) and out-of-plane (black line) line-cut profiles of GIWAXS patterns. (e) R-SoXS of three blend films.

In summary, we have designed and synthesized three indacenobis(dithieno[3,2-*b*:2′,3′-*d*]pyrrol) based NFAs with/without halogen-substituted endgroups. Chlorinated NFA exhibits a narrower optical bandgap of 1.32 eV with more intense molecular packing in comparison with fluorinated and hydrogenated substitutes, which is owing to its stronger ICT effect. Indeed, the photovoltaic performance of PBDB-T:**IPIC-4Cl** OSCs exhibited an outstanding PCE of 13.4% with extremely low energy loss (0.51 eV). The devices were further optimized by adding 30 wt% $PC_{71}BM$ as a phase

mediator to reveal a higher PCE of 14.3%. Our results indicate that the chlorination strategy is an efficient approach to design novel NFA structure to realize high performance OSCs.

ASSOCIATED CONTENT

Supporting Information

The Supporting Information is available free of charge on the ACS Publications website at DOI: 10.1021/acsenergylett.xxxxxx.

Synthesis details, NMR and mass characterization, optical, electrochemical, device characterization, mobility measurement, and comparison with literature best-performing devices data (PDF)

AUTHOR INFORMATION

Corresponding Author

*E-mail: fengliu82@sjtu.edu.cn (F. L.).
*E-mail: derya.baran@kaust.edu.sa (D. B.).
*E-mail: whtang@njust.edu.cn (W. T.).

Author Contributions

[#]R.G. and X.S. contributed equally.

Notes

The authors declare no competing financial interest

ACKNOWLEDGEMENTS

This work is financially supported by the National Natural Science Foundation of China (Grant No. 51573077, 21875111), Jiangsu Province Natural Science Foundation (BK20180496, BK20130032), the 333 Project to Cultivate High Level Talents in Jiangsu Province, Six Talent Peaks Project in Jiangsu Province, and the Priority Academic Program Development of Jiangsu Higher Education Institutions.

REFERENCES

(1) Song W.; Fan X.; Xu B.; Yan F.; Cui H.; Wei Q.; Peng R.; Hong L.; Huang J.; Ge

Z. All- Solution- Processed Metal- Oxide- Free Flexible Organic Solar Cells with Over 10% Efficiency. *Adv. Mater.* **2018**, *30*, 1800075.

(2) Lin Y.; Zhao F.; Prasad S. K. K.; Chen J. D.; Cai W.; Zhang Q.; Chen K.; Wu Y.; Ma W.; Gao F.; *et al*. Balanced Partnership between Donor and Acceptor Components in Nonfullerene Organic Solar Cells with >12% Efficiency. *Adv. Mater.* **2018**, *30*, 1706363.

(3) Bucher L.; Desbois N.; Koukaras E. N.; Devillers C. H.; Biswas S.; Sharma G. D.; Gros C. P. BODIPY–Diketopyrrolopyrrole–Porphyrin Conjugate Small Molecules for Use in Bulk Heterojunction Solar Cells. *J. Mater. Chem. A* **2018**, *6*, 8449-8461.

(4) Zhang K.; Fan B.; Xia R.; Liu X.; Hu Z.; Gu H.; Liu S.; Yip H.L.; Ying L.; Huang F.; *et al*. Highly Efficient Tandem Organic Solar Cell Enabled by Environmentally Friendly Solvent Processed Polymeric Interconnecting Layer. *Adv. Energy Mater.* **2018**, *8*, 1703180.

(5) McDowell C.; Abdelsamie M.; Toney M. F.; Bazan G. C. Solvent Additives: Key Morphology- Directing Agents for Solution- Processed Organic Solar Cells. *Adv. Mater.* **2018**, *30*, 1707114.

(6) Cheng P.; Zhan X. Stability of Organic Solar Cells: Challenges and Strategies. *Chem. Soc. Rev.* **2016**, *45*, 2544-2582.

(7) Cheng P.; Li G.; Zhan X.; Yang Y. Next-Generation Organic Photovoltaics Based on Non-Fullerene Acceptors. *Nat. Photon.* **2018**, *12*, 131-142.

(8) Fu H.; Wang Z.; Sun Y. Advances in Non- Fullerene Acceptor Based Ternary Organic Solar Cells. *Solar RRL* **2018**, *2*, 1700158.

(9) Lopez S. A.; Sanchez-Lengeling B.; Soares J.; Aspuru-Guzik A. Design Principles and Top Non-Fullerene Acceptor Candidates for Organic Photovoltaics *Joule* **2017**, *1*, 857-870.

(10) Mishra A.; Keshtov M. L.; Looser A.; Singhal R.; Stolte M.; Wurthner F.; Bauerle P.; Sharma G. D. Unprecedented Low Energy Losses in Organic Solar Cells with High External Quantum Efficiencies by Employing Non-Fullerene Electron Acceptors. *J. Mater. Chem. A* **2017**, *5*, 14887-14987.

(11) Wadsworth A.; Moser M.; Marks A.; Little M. S.; Gasparini N.; Brabec C. J.; Baran D.; McCulloch I. Critical Review of the Molecular Design Progress in Non-Fullerene Electron Acceptors towards Commercially Viable Organic Solar Cells. *Chem. Soc. Rev.* **2018**, DOI: 10.1039/c7cs00892a.

(12) Qian D.; Zheng Z.; Yao H.; Tress W.; Hopper T.; Chen S.; Li S.; Liu J.; Chen S.; Zhang J.; *et al*. Design Rules for Minimizing Voltage Losses in High-Efficiency Organic Solar Cells. *Nat. Mater.* **2018**, *17*, 703-709.

(13) Yan C.; Barlow S.; Wang Z.; Yan H.; Jen A. K. Y.; Marder S. R.; Zhan X. Non-Fullerene Acceptors for Organic Solar Cells. *Nat. Rev. Mater.* **2018**, *3*, 18003.

(14) Zhang G.; Zhao J.; Chow P. C. Y.; Jiang K.; Zhang J.; Zhu Z.; Zhang J.; Huang F.; H. Yan. Nonfullerene Acceptor Molecules for Bulk Heterojunction Organic Solar Cells. *Chem. Rev.* **2018**, *118*, 3447-3507.

(15) Yuan J.; Zhang Y.; Zhou L.; Zhang G.; Yip H.; Lau T.; Lu X.; Zhu C.; Peng H.; Johnson P.; *et al*. Single-Junction Organic Solar Cell with Over 15% Efficiency Using Fused-Ring Acceptor with Electron-Deficient Core. Joule, **2019**, *3*, 1-12.

(16) Li S.; Ye L.; Zhao W.; Yan H.; Yang B.; Liu D.; Li W.; Ade H.; Hou J. A Wide Band Gap Polymer with a Deep Highest Occupied Molecular Orbital Level Enables 14.2% Efficiency in Polymer Solar Cells. *J. Am. Chem. Soc.* **2018**, *140*, 7159-7167.

(17) Zhang H.; Yao H.; Hou J.; Zhu J.; Zhang J.; Li W.; Yu R.; Gao B.; Zhang S.; Hou J. Over 14% Efficiency in Organic Solar Cells Enabled by Chlorinated Nonfullerene Small- Molecule Acceptors. *Adv. Mater.* **2018**, *30*, 1800613.

(18) Zhang S.; Qin Y.; Zhu J.; Hou J. Over 14% Efficiency in Polymer Solar Cells Enabled by a Chlorinated Polymer Donor. *Adv. Mater.* **2018**, *30*, 1800868.

(19) Meng L.; Zhang Y.; Wan X.; Li C.; Zhang X.; Wang Y.; Ke X.; Xiao Z.; Ding L.; Xia R.; *et al*. Organic and Solution-Processed Tandem Solar Cells with 17.3% Efficiency. *Science*, **2018**, *361*, 1094-1098.

(20) Feng H.; Yi Y.; Ke X.; Zhang Y.; Wan X.;Li C.; Chen Y. Synergistic Modifications of Side Chains and End Groups in Small Molecular Acceptors for High Efficient Non-Fullerene Organic Solar Cells. *Sol. RRL* **2018**, *2*, 1800053.

(21) Su W.; Fan Q.; Guo X.; Chen J.; Wang Y.; Wang X.; Dai P.; Ye C.; Bao X.; Ma W.; *et al*. Significant Enhancement of Photovoltaic Performance of Organic Small Molecule Acceptor via Side-Chain Engineering. *J. Mater. Chem. A* **2018**, *6*, 7988-7996.

(22) Kan B.; Feng H.; Yao H.; Chang M.; Wan X.; LiC.; Hou J.; Chen Y. A Chlorinated Low-Bandgap Small-Molecule Acceptor for Organic Solar Cells with 14.1% Efficiency and Low Energy Loss. *Sci. China Chem.* **2018**, 61, 1307-1313.

(23) Awartani O.; Gautam B.; Zhao W.; Younts R.; Hou J.; Gundogdu K.; Ade H. Polymer Non-Fullerene Solar Cells of Vastly Different Efficiencies for Minor Side-Chain Modification: Impact of Charge Transfer, Carrier Lifetime, Morphology and Mobility. *J. Mater. Chem. A* **2018**, *6*, 12484-12492.

(24) Bin H.; Yao J.; Yang Y.; Angunawela I.; Sun C.; Gao L.; Ye L.; Qiu B.; Xue L.; Zhu C.; *et al*. High- Efficiency All- Small- Molecule Organic Solar Cells Based on an Organic Molecule Donor with Alkylsilyl- Thienyl Conjugated Side Chains. *Adv. Mater.* **2018**, *30*, 1706361.

(25) Chen S.; Lee S. M.; Xu J.; Lee J.; Lee K. C.; Hou T.; Yang Y.; Jeong M.; Lee B.; Cho Y.; *et al*. Ultrafast Channel II Process Induced by A 3-D Texture with Enhanced Acceptor Order Ranges for High-Performance Non-Fullerene Polymer Solar Cells. *Energy Environ. Sci.***2018**, *11*, 2569-2580.

(26) Guo B.; Li W.; Guo X.; Meng X.; Ma W.; Zhang M.; Li Y. High Efficiency Nonfullerene Polymer Solar Cells with Thick Active Layer and Large Area. *Adv. Mater.* **2017**, *29*, 1702291.

(27) Xu X.; Li Z.; Bi Z.; Yu T.; Ma W.; Feng K.; Li Y.; Peng Q. Highly Efficient Nonfullerene Polymer Solar Cells Enabled by a Copper(I) Coordination Strategy Employing a 1,3,4- Oxadiazole- Containing Wide- Bandgap Copolymer Donor. *Adv. Mater.* **2018**, *30*, 1800737.

(28) Cui Y.; Yang C.; Yao H.; Zhu J.; Wang Y.; Jia G.; Gao F.; Hou J. Efficient Semitransparent Organic Solar Cells with Tunable Color enabled by an Ultralow-Bandgap Nonfullerene Acceptor. *Adv. Mater*. **2017**, 29, 1703080.

(29) Wang Y.; Zhang Y.; Qiu N.; Feng H.; Gao H.; Kan B.; Y Ma.; Li C.; Wan X.; Chen Y. A Halogenation Strategy for over 12% Efficiency Nonfullerene Organic Solar Cells. *Adv. Energy Mater*. 2018, 8, 1702870.

(30) Chen Y.; Liu T.; Hu H.; Ma T.; Lai J. Y. L.; Zhang J.; Ade H.; Yan H. Modulation of End Groups for Low- Bandgap Nonfullerene Acceptors Enabling High-Performance Organic Solar Cells. *Adv. Energy Mater.* 2018, 8, 1801203.

(31) Li Y.; Lin J. D.; Che X.; Qu Y.; Liu F.; Liao L. S.; Forrest S. R. High Efficiency Near-Infrared and Semitransparent Non-Fullerene Acceptor Organic Photovoltaic Cells. J. Am. Chem. Soc. 2017, 139, 17114-17119.

(32) Sun J.; Ma X.; Zhang Z.; Yu J.; Zhou J.; Yin X.; Yang L.; Geng R.; Zhu R.; Zhang F.; *et al*. Dithieno [3, 2-*b*:2′, 3′-*d*] pyrrol Fused Nonfullerene Acceptors Enabling Over 13% Efficiency for Organic Solar Cells. *Adv. Mater.* **2018**, *30*, 1707150.

(33) Ma X.; Gao W.; Yu J.; An Q.; Zhang M.; Hu Z.; Wang J.; Tang W.; Yang C.; Zhang F. Ternary Nonfullerene Polymer Solar Cells with Efficiency> 13.7% by Integrating the Advantages of Materials and Two Binary Cells. *Energy Environ. Sci.* **2018**, *11*, 2134-2141.

(34) Li, W.; Cheng, M.; Zhang, Z.; Cai, J.; Zhang, H.; Gurney, R. S.; Liu, D.; Yu, J.; Tang, W.; Wang, T. Retarding the Crystallization of A Non-Fullerene Electron-Acceptor for High Performance Polymer Solar Cells. *Adv. Funct. Mater.* **2018**, *28*, 1807662.

(35) Song X.; Gasparini N.; Ye L.; Yao H.; Hou J.; Ade H.; Baran D. Controlling Blend Morphology for Ultrahigh Current Density in Nonfullerene Acceptor Based

Organic Solar Cells. *ACS Energy Lett*. **2018**, *3*, 669-676.

(36) Zhang Y.; Yao H.; Zhang S.; Qin Y.; Zhang J.; Yang L.; Li W.; Wei Z.; Gao F.; Hou J. Fluorination vs. Chlorination: A Case Study on High Performance Organic Photovoltaic Materials. *Sci. China Chem*. **2018**, *61*, 1328-1337.

(37) Yang Y.; Chen W.; Dou L.; Chang W.; Duan H.; Bob B.; Li G.; Yang Y. High-Performance Multiple-Donor Bulk Heterojunction Solar Cells. Nat. Photonics **2015**, *9*, 190-198.

(38) Zhou Z.; Xu S.; Song J.; Jin Y.; Yue Q.; Qian Y.; Liu F.; Zhang F.; Zhu X. High-Efficiency Small-Molecule Ternary Solar Cells with A Hierarchical Morphology Enabled by Synergizing Fullerene and Non-Fullerene Acceptors. *Nat. Energy* **2018**, *3*, 952-959.

(39) Chao P.; Mu Z.; Wang H.; Mo D.; Chen H.; Meng H.; Chen W.; He F. Chlorination of Side Chains: A Strategy for Achieving a High Open Circuit Voltage Over 1.0 V in Benzo[1,2-b:4,5-b′]dithiophene-Based Non-Fullerene Solar Cells. *ACS Appl. Energy Mater.* **2018**, *1*, 2365-2372.

(40) Li X.; Yan T.; Bin H.; Han G.; Xue L.; Liu F.; Yi Y.; Zhang Z.; Russelle T.; Li Y. Insertion of Double Bond π-Bridges of A-D-A Acceptors for High Performance Near-Infrared Polymer Solar Cells. *J. Mater. Chem. A* **2017**, *5*, 22588-22597.

(41) Gao W.; An Q.; Zhong C.; Luo Z.; Ming R.; Zhang M.; Zou Y.; Liu F.; Zhang F.; Yang C. Designing An Asymmetrical Isomer to Promote the LUMO Energy Level and Molecular Packing of A Non-Fullerene Acceptor for Polymer Solar Cells with 12.6% Efficiency. *Chem. Sci.* **2018**, *9*, 8142-8149.

(42) Li W.; Ye L.; Li S.; Yao H.; Ade H.; Hou J. A High-Efficiency Organic Solar Cell Enabled by the Strong Intramolecular Electron Push-Pull Effect of the Nonfullerene Acceptor. *Adv. Mater.* **2018**, *30*, 1707170.

(43) Xiao Z.; Jia X.; Ding L. Ternary Organic Solar Cells Offer 14% Power Conversion Efficiency. *Sci. Bull.* **2017**, *62*, 1562-1564.

(44) Huang W.; Cheng P.; Yang Y.; Li G.; Yang Y. High-Performance Organic Bulk-Heterojunction Solar Cells Based on Multiple-Donor or Multiple-Acceptor Components. *Adv. Mater.* **2018**, *30*, 1705706.

(45) Zhang J.; Liu F.; Chen S.; Yang C.; Zhu X.; Zhu D. High-Performance Polymer Solar Cells Achieved by Introducing Side-Chain Heteroatom on Small-Molecule Electron Acceptor. *Macromol. Rapid Commun.* **2018**, *39*, 1800393.

(46) Huang C.; Liao X.; Gao K.; Zuo L.; Lin F.; Shi X.; Li C.; Liu H.; Li X.; Liu F.; *et al*. Highly Efficient Organic Solar Cells Based on S,N-Heteroacene Non-Fullerene Acceptors. *Chem. Mater.* **2018**, *30*, 5429-5434.

(47) Luo Z.; Zhao Y.; Zhang Z.; Li G.; Wu K.; Xie D.; Gao W.; Li Y.; Yang C. Side-Chain Effects on Energy-Level Modulation and Device Performance of Organic Semiconductor Acceptors in Organic Solar Cells. *ACS Appl. Mater. Interfaces* **2017**, *9*, 34146-34152.

(48) Liu X.; Xie B.; Duan C.; Wang Z.; Fan B.; Zhang K.; Lin B.; Colberts F.; Ma W.; Janssen R.; *et al*. a High Dielectric Constant Non-Fullerene Acceptor for Efficient Bulk-Heterojunction Organic Solar Cells. *J. Mater. Chem. A* **2018**, *6*, 395-403.

(49) Privado M.; Cruz P.; Biswas S.; Singhal R.; Sharma G.; Langa F. A Non-Fullerene All

Small Molecule Solar Cell Constructed with A Diketopyrrolopyrrole-Based Acceptor Having a Power Conversion Efficiency Higher than 9% and an Energy Loss of 0.54 eV. *J. Mater. Chem. A,* **2018**, *6*, 11714-11724.

(50) Yang Y.; Wang J.; Xu H.; Zhan X.; Chen X. Nonfullerene Acceptor with "Donor Acceptor Combined π-Bridge" for Organic Photovoltaics with Large Open-Circuit Voltage. *ACS Appl. Mater. Interfaces* **2018**, *10*, 18984-18992.

(51) Fan Q.; Zhu Q.; Xu Z.; Su W.; Chen J.;Wu J.; Guo X.; Ma W.; Zhang M.; Li Y. Chlorine Substituted 2D-Conjugated Polymer for High-Performance Polymer Solar Cells with 13.1% Efficiency via Toluene Processing. *Nano Energy* **2018**, *48*, 413-420.

(52) Zhang H.; Zhang S.; Gao K.; Liu F.; Yao H.; Yang B.; He C.; Russell T.; Hou J. Low Band-Gap Conjugated Polymer Based on Diketopyrrolopyrrole Units and Its Application in Organic Photovoltaic Cells. *J. Mater. Chem. A* **2017**, *5*, 10416-10423.

(53) Zhang H.; Wang X.; Yang L.; Zhang S.; Zhang Y.; He C.; Ma W.; Hou J. Improved Domain Size and Purity Enables Efficient All-Small-Molecule Ternary Solar Cells. *Adv. Mater.* **2017**, *29*, 1703777.

(54) Ye L.; Hu H.; Ghasemi M.; Wang T.; Collins B.; Kim J.; Jiang K.; Carpenter J.; Li H.; Li Z.; *et al*. Quantitative Relations Between Interaction Parameter, Miscibility and Function in Organic Solar Cells. *Nat. Mater.* **2018**, *17*, 253-260.